

## Rapid and On-site Detection of Uranyl Ions via Ratiometric Fluorescence Signals Based on a Smartphone Platform

*Xinfeng Chen<sup>a, ||</sup>, Qingsong Mei<sup>b, ||</sup>, Long Yu<sup>a</sup>, Hongwei Ge<sup>a</sup>, Ji Yue<sup>a</sup>, Kui Zhang<sup>c, \*</sup>, Tasawar Hayat<sup>d</sup>, Ahmed Alsaedi<sup>d</sup>, and Suhua Wang<sup>a, \*</sup>*

<sup>a</sup>College of Environmental Science and Engineering, North China Electric Power University, Beijing, 102206, China

<sup>b</sup>School of Biological and Medical Engineering, Hefei University of Technology, Hefei, Anhui, 230009, China

<sup>c</sup>School of Chemistry and Chemical Engineering, Anhui University of Technology, Ma'anshan, Anhui 243032, China

<sup>d</sup>NAAM Research Group, King Abdulaziz University, Jeddah 21589, Saudi Arabia

\* Corresponding author: wangshuhua@ncepu.edu.cn; zhangkui@mail.ustc.edu.cn

|| These authors contributed equally to this work

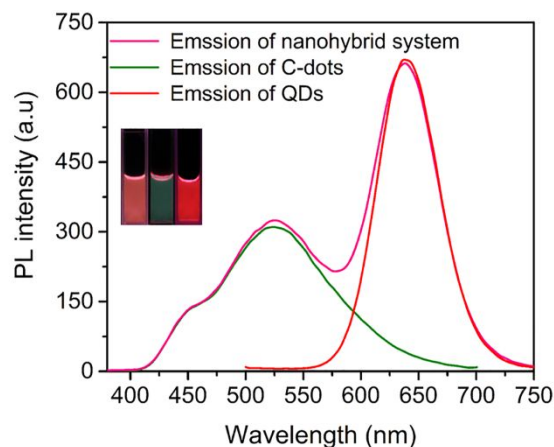


**Fig. S1** Fluorescent emission spectra of MPA@CdTe QDs (red line), C-dots (green line) and the ratiometric probe.

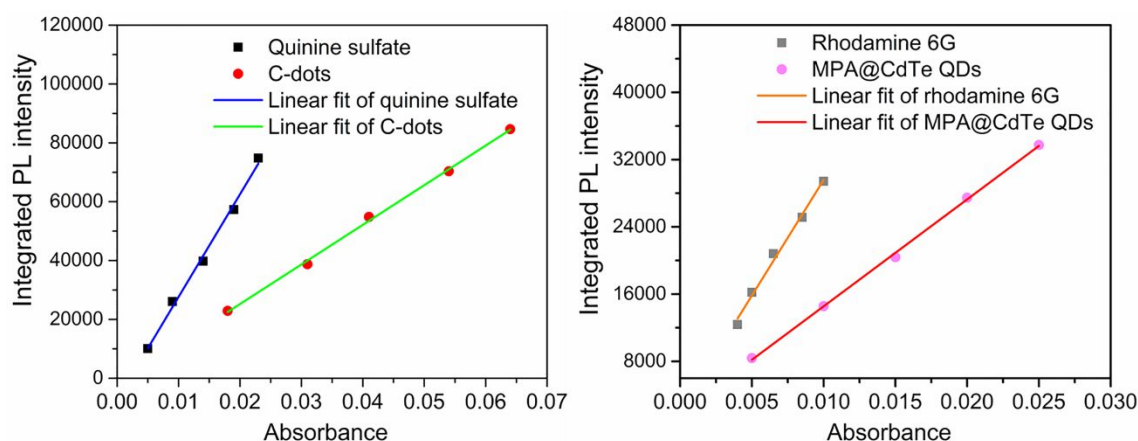


**Fig. S2** Determination of the fluorescence quantum yields of the C-dots (left) and MPA@CdTe QDs (right) using quinine sulfate and rhodamine 6G as standard respectively.

The fluorescence quantum yields of C-dots and MPA@CdTe were using the following equation:

$$\Phi_{sample} = \Phi_{standard} \cdot \frac{Grad_{sample}}{Grad_{standard}} \cdot \frac{\eta_{sample}^2}{\eta_{standard}^2}$$

Herein,  $\Phi$  is the fluorescence quantum yield, Grad represents the slope of the plot of absorbance at the excitation wavelength versus the measured integrated PL intensity (area), and  $\eta$  is the refractive index of the solvent used. The quinine sulfate in 0.1M sulfuric acid at 360nm excitation ( $\Phi_F = 0.56$ ) and rhodamine 6G in ethanol solution at 400 nm ( $\Phi_F = 0.95$ ) were selected as the standard for C-dots and MPA@CdTe respectively. Based on this method, the quantum yield of the C-dots and MPA@CdTe were calculated to be 21.62% and 42.15% respectively.

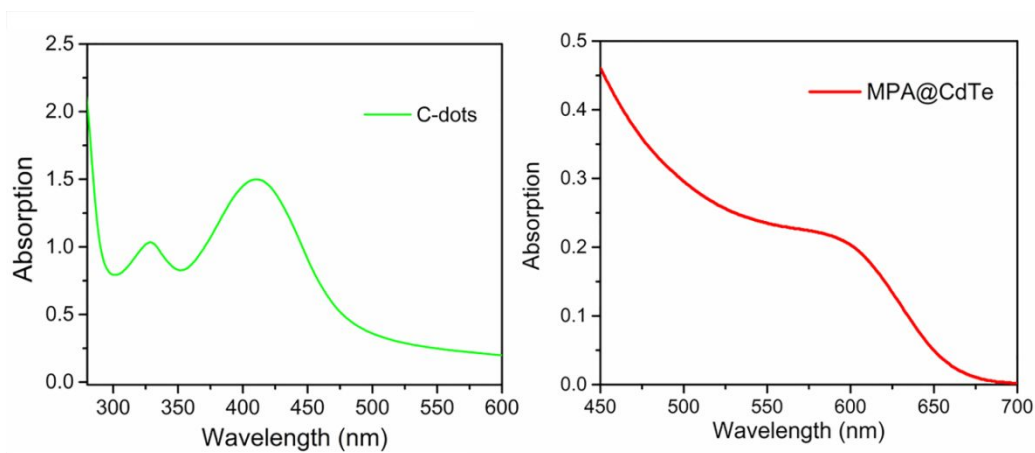


**Fig. S3** UV-vis absorption spectra of C-dots (left) and MPA@CdTe QDs (right). The absorption peak of C-dots is located at 410 nm and the solution color is primrose yellow. For the QDs of MPA@CdTe, an absorption maximum of the first electronic transition at 600 nm can be observed, indicating a sufficiently narrow size distribution of the QDs.

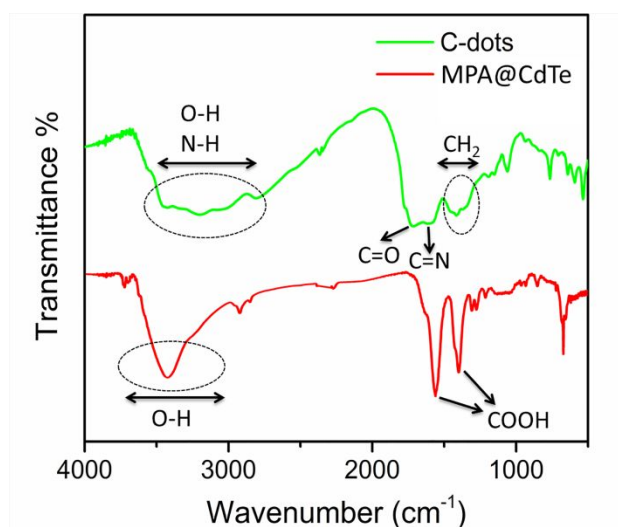


**Fig. S4** The Fourier transformed infrared (FT-IR) spectra of the C-dots (green line) and MPA@CdTe (red line) samples.

The function group on the surface of C-dots and MPA@CdTe QDs were detected by using FT-IR, the FT-IR spectrum of C-dots shows a broad absorption bands at 3000~3552  $\text{cm}^{-1}$  are attributed to  $\nu(\text{N-H})$  and  $\nu(\text{O-H})$ . Absorption bands at 1640~1780  $\text{cm}^{-1}$  are assigned to  $\nu(\text{C=O})$ , and absorption bands at 1550~1630  $\text{cm}^{-1}$  are assigned to  $\nu(\text{C=N})$ . These functional groups improve hydrophilicity and stability of the C-dots in aqueous. Absorption bands from 1350~1460  $\text{cm}^{-1}$  are assigned to  $\delta(\text{CH}_2)$ . For MPA@CdTe, the absorption peaks at 3430  $\text{cm}^{-1}$  can be assigned to the stretching vibrations of hydroxy group (-OH), the peaks at 1385  $\text{cm}^{-1}$  and 1564  $\text{cm}^{-1}$  can be attributed to symmetrical stretching vibrations and asymmetrical stretching vibrations of carboxylate anion ( $\text{COO}^-$ ) respectively, indicating the MPA molecules were modified on the surface of CdTe QDs. Besides, there is no stretching vibrations peaks of sulfhydryl group (-SH) at 2500~2600  $\text{cm}^{-1}$ , further proved the MPA molecules bind to the surface of QDs by coordination.

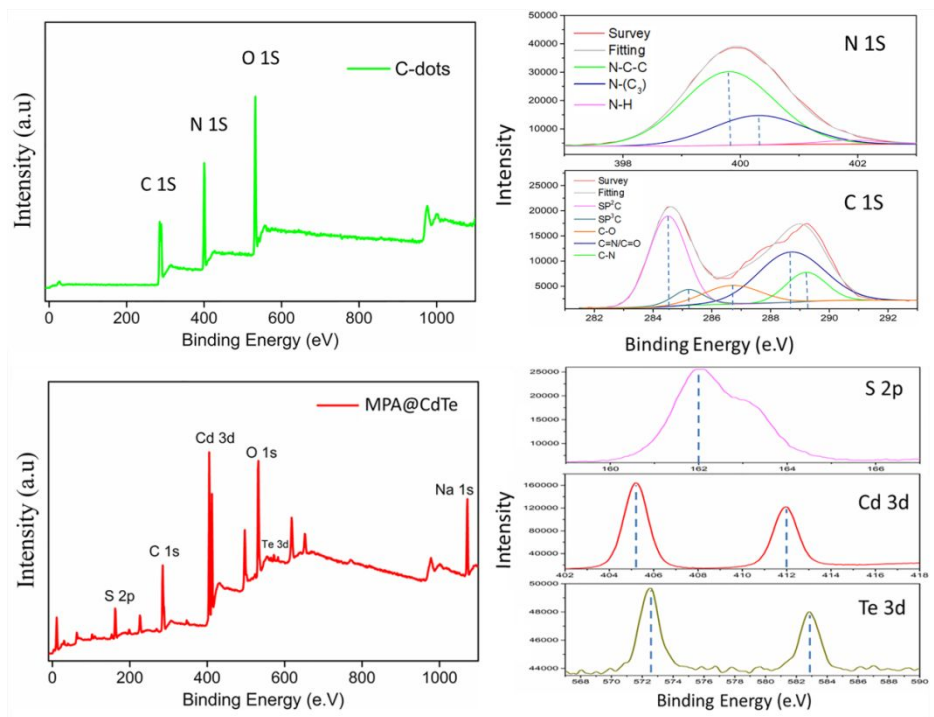


**Fig. S5** XPS data of C-dots (top) and CdTe@MPA QDs (bottom). The element composition and surface analysis for C-dots and MPA@CdTe were further performed by XPS.

The XPS spectra of C-dots show three peaks at 284.0, 400.0, and 530.6 eV, which are assigned to C1s, N1s, and O1s, respectively. The N1s spectrum can be deconvoluted into 399.8, 400.3, and 401.9 eV, which are attributed to the C–N–C, N–(C)<sub>3</sub>, and N–H bands, respectively. The C1s spectrum can be deconvoluted into 284.5 eV, 285.2 eV, 286.7 eV, 288.7 eV and 289.2 eV, which are assigned to SP<sup>2</sup>C, SP<sup>3</sup>C, C–O, C=N/C=O, C–N. For MPA@CdTe spectrum, Cd, Te together with C, S, O elements can be detected. In the high resolution spectrum, the binding energies of 405.2 eV and 412 eV correspond to the Cd 3d levels, and binding energy of 572.6 eV and 582.9 eV can be assigned to Te 3d levels. The binding energy of 162 eV represents S 2P, which is resulted from the coordination between S and Cd. The relatively high content of Cd and S compared to Te confirmed the formation of CdS-rich shell in the surface of QDs, which is consistent with the results of XRD examination and previous reports.

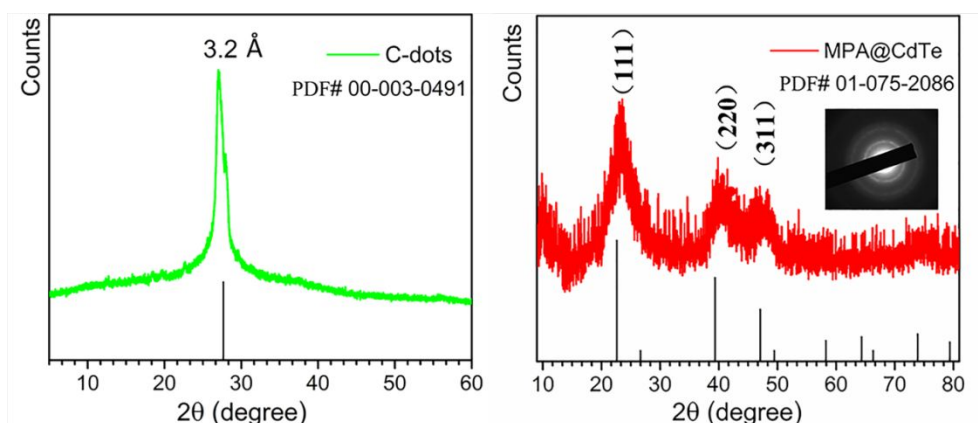


**Fig. S6** The XRD patterns of the C-dots (left) and MPA@CdTe (right) samples. As can be seen in Figure 4, the strong diffraction peak of C-dots centered at 28.5 can be attributed to the diffraction of (002) lattice planes of graphitic carbon.

For MPA@CdTe QDs samples, the three diffraction peaks can be assigned to (111), (220) and (311) lattice planes according to the card of 01-075-2086. The slight shift of the diffraction peaks can be attributed to the formation of CdS-rich shell on the surface of QDs. The broadening diffraction peaks suggest a small size of the crystalline QDs. Furthermore, the selected area electron diffraction pattern of the QDs shows clear diffraction ring which can be indexed as cubic (zinc blende) structure of QDs.

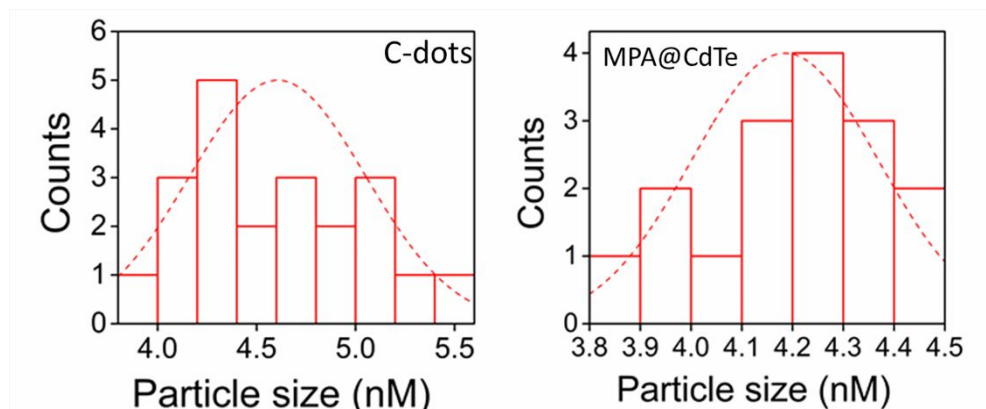


**Fig. S7** The size distribution and histograms of the C-dots (left) and MPA@CdTe QDs (right) prepared in this work. The averaged sizes are 4.5 nm and 4.3 nm.

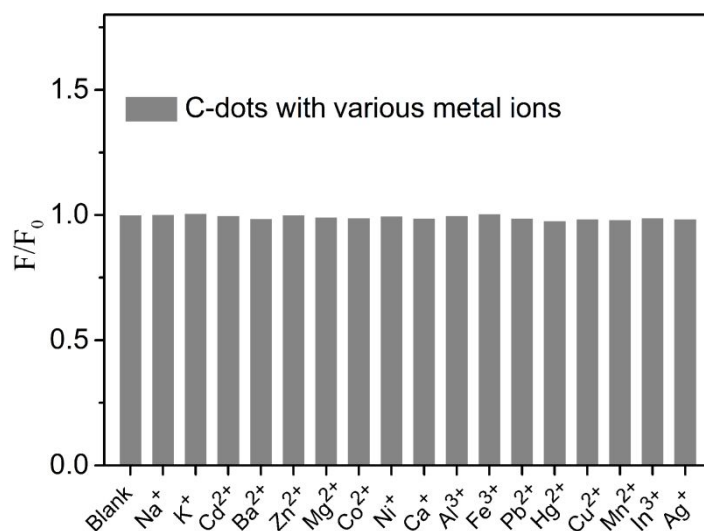


**Fig. S8** The fluorescence response of C-dots to possible interfering metal ions, clearly, these metal ions have no any effect on the fluorescence of C-dots.

**Table S1** The summary and comparison of the synthetic method and fluorescence properties among the C-dots synthesized in this work and previously reported.

Previous work	Synthetic material and conditions	$\lambda_{\text{max}}$ / ions
Journal of Alloys and Compounds, 2017, 701, 75-81	Citric acid (1 g), urea (2 g), DMF solution (10 mL); Teflon-lined autoclave and heated at 200 °C / 6h	Max $\lambda_{\text{em}}$ =523 nm Cu, Ag,
Journal of Luminescence, 2016, 175, 129-134.	Citric acid (0.21 g) and urea (0.18 g) water (5mL) Teflon-lined autoclave and heated at 160 °C/ 4h	Max $\lambda_{\text{em}}$ =450 nm Hg
Ecotoxicology and Environmental Safety, 2018, 153, 101-106.	Citric acid (1 g), urea (1 g) and thiourea (1 g) irradiated for 5 min in a microwave oven at 450 W	Max $\lambda_{\text{em}}$ =300~550 nm Hg
Nanoscale, 2015, 48, 20743-20748.	Citric acid (1.051 g) and ethylenediamine (335 $\mu$ L); into deionized water (10 mL) atmosphere-pressure microplasma	Max $\lambda_{\text{em}}$ =416~547 nm pH /Uranium
Our work	Citric acid (1 g) and urea (3 g) and deionized water (10 mL) , flowing air, 200 °C/3 h	No available

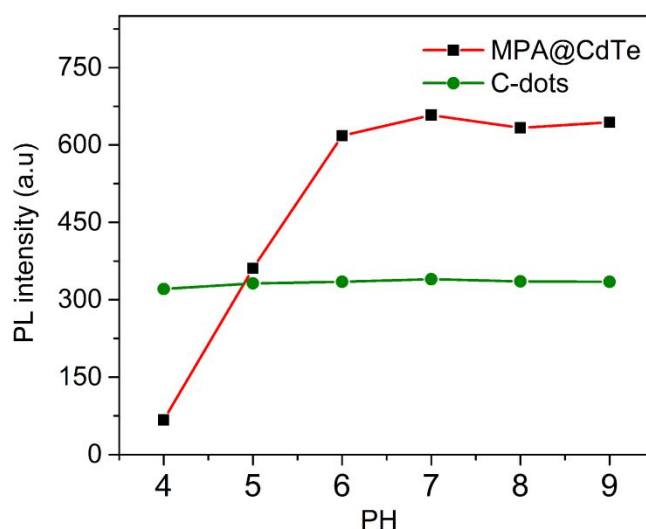


**Fig. S9** The fluorescence intensities of MPA@CdTe QDs (red line) and C-dots (green line) in different pH conditions.

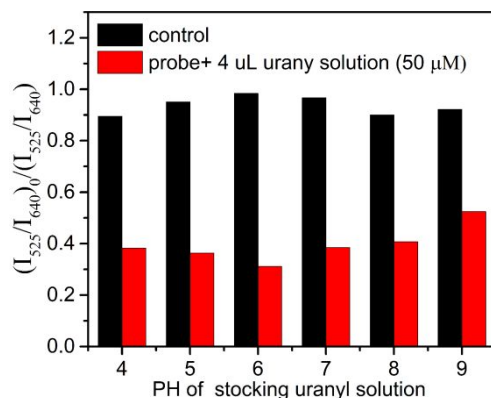


**Fig. S10** The fluorescence intensity of the probe solution (2 mL) before and after the addition of uranyl solution with different pH values (20  $\mu$ L). The pH of control and uranyl stocking solution was adjusted by 0.1 M HNO<sub>3</sub> and NaOH.

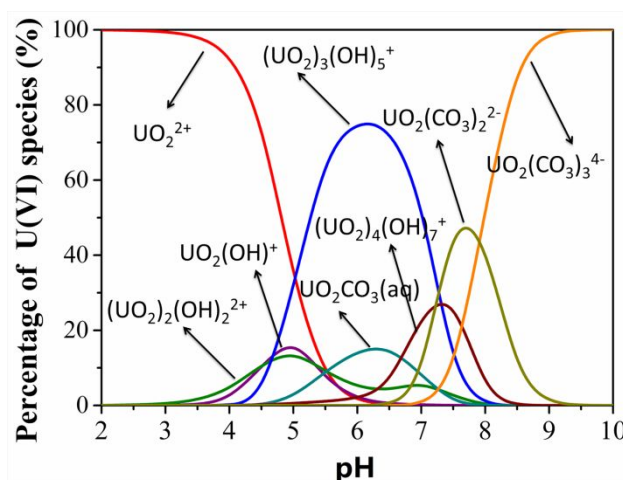


**Fig. S11** The pH-dependence of various U(VI) species in aqueous solution. T = 293 K,  $C_{U(VI)initial} = 5.0 \times 10^{-5}$  mol L<sup>-1</sup>, I = 0.01 mol L<sup>-1</sup> NaNO<sub>3</sub>; (Reference: *ACS Sustainable Chemistry & Engineering*, 2017, 5 (4), pp 3583–3595).

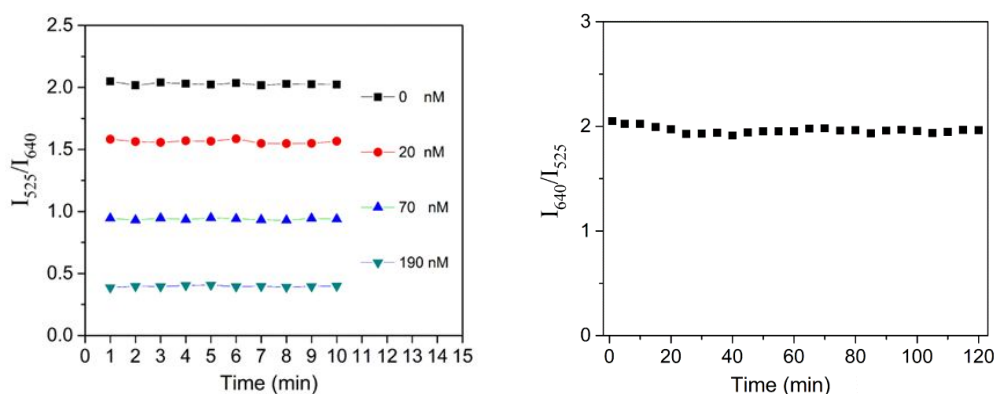


**Fig. S12** The kinetics of the response of ratiometric probe to uranyl ions within 15 min (left). The photostability of ratiometric probe in water against consecutive illumination (pulse irradiation time recorded every five minutes in two hours) (right)



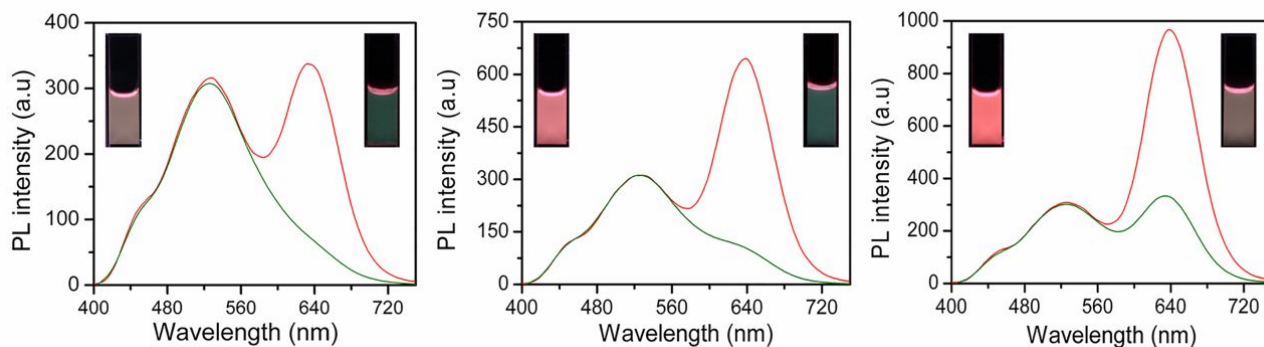


**Fig. S13** The color changes of the ratiometric probe responses to a fixed amount of uranyl ions under the intensity ratio ( $I_{525}/I_{640}$ ) of 1:1 (left), 1:2 (center) and 1:3 (right), respectively.

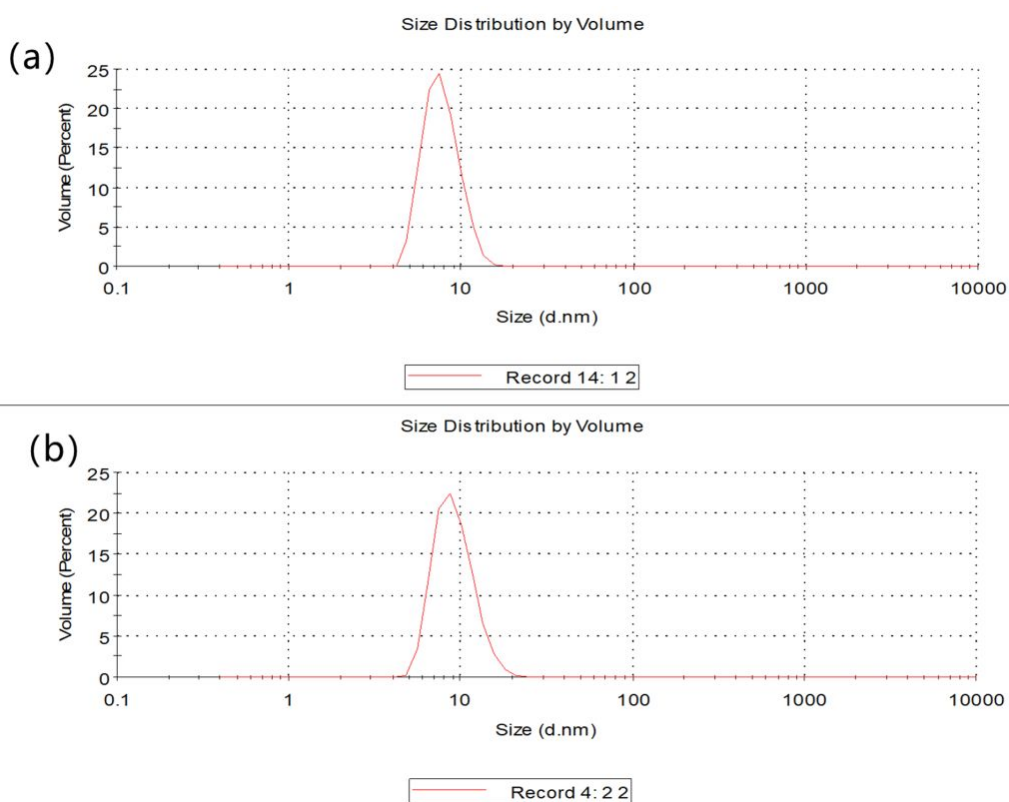


**Fig. S14.** The dynamic light scattering of MPA@CdTe QDs before (a) and after reaction with uranyl ions (b) respectively.



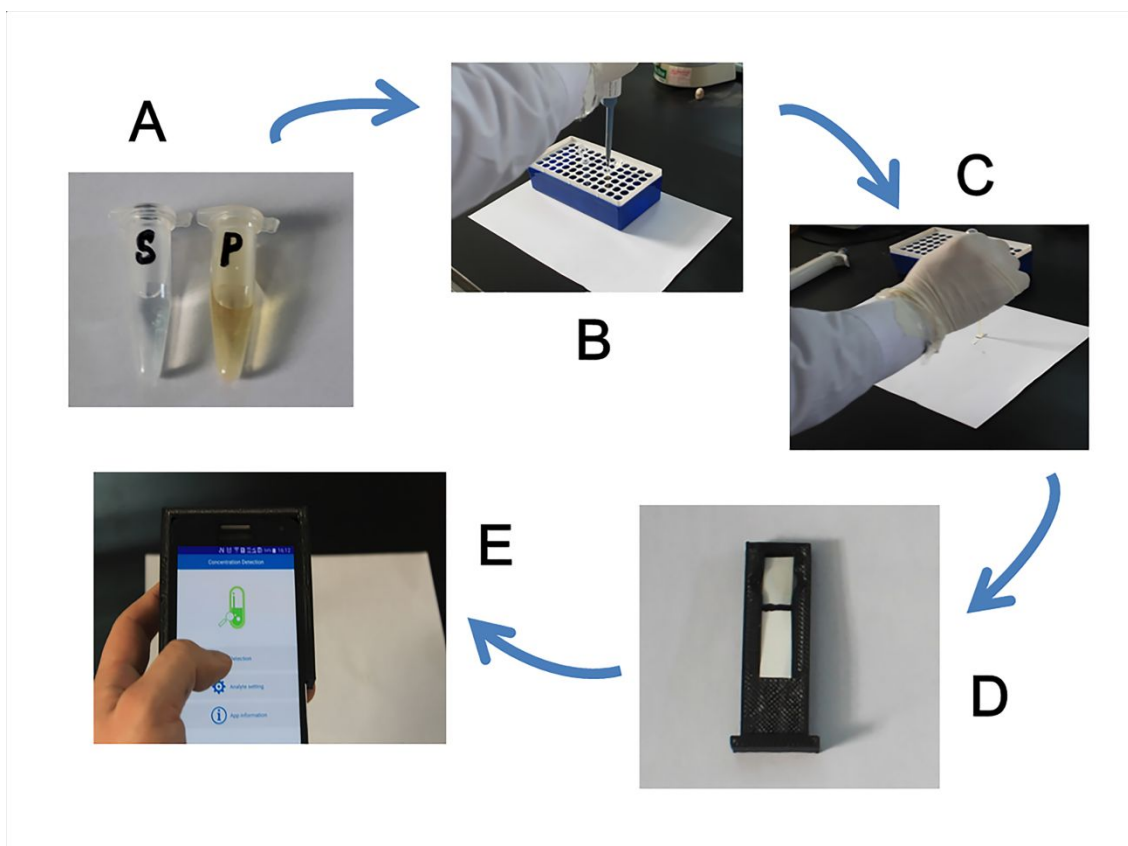


**Fig. S15** Steps for detecting uranyl ions by using of smartphone-based platform. (A) The real sample (“S”) and probe (“P”) solution; (B) Drop the sample into the probe solution; (C) Deposited the mixture solution on strip; (D) Put the strip in slot; (E) Recognition.

**Table S2** Spike and recovery study of smartphone-based detection system in different real water samples.

Add uranyl ions Concentration ( $\mu\text{M}$ )	Lake water		Tap water		Mineral water	
	Found ( $\mu\text{M}$ )	Recovery (%)	Found ( $\mu\text{M}$ )	Recovery (%)	Found ( $\mu\text{M}$ )	Recovery (%)
2	2.5	80%	2.5	80%	2.5	80%
50	50	100%	50	100%	50	100%
85	90	94.4%	90	94.4%	90	94.4%